This document is downloaded from the
VTT's Research Information Portal
https://cris.vtt.fi

VTT Technical Research Centre of Finland

Sensitivity of the Master Curve reference temperature T0 to the crack front curvature

Lindqvist, Sebastian; Kuutti, Juha

Published in:
Theoretical and Applied Fracture Mechanics

DOI:
10.1016/j.tafmec.2022.103558

Published: 01/12/2022

Document Version
Publisher's final version

License
CC BY

Link to publication

Please cite the original version:
Lindqvist, S., & Kuutti, J. (2022). Sensitivity of the Master Curve reference temperature T0 to the crack front curvature. *Theoretical and Applied Fracture Mechanics*, *122*, [103558]. https://doi.org/10.1016/j.tafmec.2022.103558

VTT
http://www.vtt.fi
P.O. box 1000FI-02044 VTT
Finland

By using VTT's Research Information Portal you are bound by the following Terms & Conditions.

I have read and I understand the following statement:

This document is protected by copyright and other intellectual property rights, and duplication or sale of all or part of any of this document is not permitted, except duplication for research use or educational purposes in electronic or print form. You must obtain permission for any other use. Electronic or print copies may not be offered for sale.

Download date: 11. Dec. 2022

Theoretical and Applied Fracture Mechanics 122 (2022) 103558

Contents lists available at ScienceDirect

Theoretical and Applied Fracture Mechanics

journal homepage: www.elsevier.com/locate/tafmec

Sensitivity of the Master Curve reference temperature T_0 to the crack front curvature

S. Lindqvist *, J. Kuutti

VTT, Kemistintie 3, 02660 Espoo, Finland

ARTICLE INFO

Keywords:
Fracture toughness
ASTM E1921
Ductile-to-brittle transition
Crack front curvature

ABSTRACT

ASTM E1921 is a testing standard to determine the fracture toughness for ferritic steels in the ductile-to-brittle transition range. If the crack front curvature criterion in the standard is not fulfilled, the result is invalid, and more testing is required. However, previous investigations do not focus on quantifying the effect of curvature on Master Curve reference temperature, T_0. The numerical and experimental analyses done in this study indicate that, for increasing crack front curvatures, the effect of curvature on T_0 is marginal and the obtained T_0 tends to provide a conservative estimate. Future investigations on large experimental data sets with the methods provided in this study would help to quantify the trends more in detail. The results contribute to the development of more cost-efficient testing methods and impact long-term operation of nuclear power plants.

1. Introduction

The development of fracture mechanics-based characterization methods in the ductile-to-brittle transition region has long been governed by the needs of the nuclear energy industry, where the availability of testing material in surveillance programs is restricted. Sub-sized and miniature specimen testing techniques have been developed to obtain directly applicable results based on fracture mechanics. This development includes validation of 5 × 10 SE(B) (single edge bend specimens with a width, W, of 10 mm and thickness, B, of 5 mm) combined with reconstitution technology, and the development and validation of 4 × 8C(T) (compact tension specimens with W = 8 mm and B = 4 mm) specimens to determine the reference temperature for the ductile-to-brittle transition region [1-5].

The key-enabling technology for miniature specimens is the Master Curve concept based on the observation that for ferritic steels a statistical, micro-mechanism based, dependence describes the scatter of fracture toughness in the ductile-to-brittle transition region, and that for ferritic steels the toughness follows a characteristic temperature dependence. The Master Curve enables determination of the reference temperature, T_0, for ductile-to-brittle transition region using 6–12 specimens. The reference temperature is defined from the Master Curve temperature dependence at 100 MPa$\sqrt{m}$ [6,7]. The method is part of ASTM E1921 specifying the specimen capacity limit and the specimen dimensions in relation to the W.

One challenge with miniature specimens is to pre-fatigue a straight enough crack front [8]. The stress state ahead of the crack along the crack front tends to promote fatigue crack growth at the centre of the specimen, and the resulting crack front is parabolic. In addition, the residual stress state, variation in material properties or machining alignment can cause uneven crack growth on the two sides resulting in a slanted crack front.

For curved crack fronts, the variations in the J-integral and constraint along the crack front can differ from a straight crack, which is the assumption the equations in ASTM E1921 are built on. The varying parameters along the crack front affect the failure probability of the specimen [9]. A curved crack front also affects the compliance of the specimen. Therefore, a crack front straightness requirement is required.

In ASTM E1921-21, "Standard test method for determination of reference temperature, T_0, for ferritic steels in the transition range", the crack front curvature as defined (by the authors) as a form of a general equation reads:

$$C = \frac{\max|a_0 - a_i|}{(b_0 B_N)^{0.5}}, \tag{1}$$

where the maximum absolute difference between the average pre-crack length, a_0, and any of the seven innermost physical pre-crack lengths, a_i with i = 2 to 8, is normalized by the square root of the remaining ligament, b_0 (=W-a_0), where W is the width of the specimen times B_N, the

* Corresponding author. Tel.: +358 4013872.
E-mail addresses: Sebastian.lindqvist@vtt.fi (S. Lindqvist), Juha.kuutti@vtt.fi (J. Kuutti).

https://doi.org/10.1016/j.tafmec.2022.103558
Received 6 May 2022; Received in revised form 23 August 2022; Accepted 23 August 2022
Available online 7 September 2022
0167-8442/© 2022 The Authors. Published by Elsevier Ltd. This is an open access article under the CC BY license (http://creativecommons.org/licenses/by/4.0/).

net thickness. The average pre-crack length is determined at nine different locations along the crack front [7]. The outermost crack length measurements are taken close to the root of the side-grooves and the other measurements are equally spaced in-between. The maximum relative curvature, C, allowed in ASTM E1921-21 is 0.1.

The curvature requirement has changed during the past years. In the ASTM E1921-20 version, the requirement is more stringent and evaluated by checking all nine physical pre-crack length measures [10]. For a typical 4 × 8C(T) specimen with $a_0/W = 0.5$, i.e. a miniature specimen, this means that a 0.36 mm difference between average pre-crack length and any crack front measurement causes invalidity of the test result and more material is needed to get enough valid results for determination of the transition temperature.

Few investigations focus on how crack front curvature affects the fracture toughness and the reference temperature T_0. Based on results for SE(B) specimens [11], a relative curvature of 0.1 affects the compliance by 10 % compared to a straight crack. M. Lambrecht et al. [8] investigated experimentally the effect of curvature on reference temperatures obtained with miniature C(T) specimens. They observe a negligible effect of crack front straightness on T_0 by comparing T_0 values based on valid and invalid crack front curvatures defined according to ASTM E1921-18 [12]. They also suggested discarding the outermost points from the crack curvature assessment, which has later been adopted by ASTM E1921-21, as described above. Yet, previous investigations do not directly quantify the effect of curvature on the reference temperature. Further work is also required to evaluate how accurate the equations in fracture toughness testing standards, e.g. ASTM E1921, are to estimate experimentally the J-integral for a curved crack front in a C(T) specimen.

In this study, the effect of crack front curvature on the reference temperature $T_0$is investigated using numerical and experimental methods. A miniature C(T) specimen is used as a reference case. Finite element analyses are applied to obtain the local J-integral and constraint profiles along the crack front for different levels of curvature, which are needed to quantify the effect of curvature on failure probability, and consequently on T_0. The simulation trends are validated by investigating experimental data sets with varying curvature. The investigated materials are ferritic steels representative of reactor pressure vessel shell materials. Finally, to assess the applicability of the formulae in ASTM E1921 for curved crack fronts, the simulated J-integrals are compared to the ones estimated based on ASTM E1921.

The results provide tools to quantify and estimate the effect of curvature on the reference temperature, which helps to understand the limitations of large crack front curvatures and develop more functional curvature criteria. The numerical results are indicative, and future investigations should focus on investigating large experimental data sets more in detail with the methods presented in this study. The results contribute to more efficient use of test material and specimens, improving the cost-effectiveness of the testing method.

2. Numerical methods and results

2.1. Specimen and crack shape assumptions

The effect of crack front curvature on the local J-integral and constraint distribution was studied on a side-grooved miniature C(T) specimen model with straight, slanted and parabolic crack fronts, as illustrated in Fig. 1. Dimensions are: $a_0 = 4$ mm, $b_0 = 4$ mm, $W = 8$ mm, and $B_N = 3.2$ mm. The crack length to width ratio is $a_0/W = 0.5$ for the straight crack (Fig. 1a). The crack front of the slanted crack (Fig. 1b) varies linearly around the mid-thickness of the specimen where $a_0/W = 0.5$. The parabolic crack front (Fig. 1c) was defined to be symmetric around $a_0/W = 0.5$, prior to application of the side grooves, with relative crack length of $a_{surface}/W = 0.42$ on the surfaces and $a_{mid}/W = 0.54$ at mid-thickness. After adding the side grooves, the crack depth of the surface points is $a_{surface}/W = 0.46$. The analyzed cases are listed in Table 1.

In Table 1, the M-parameter, the normalized inverse loading parameter, is defined as:

$$M = \frac{b_0 \sigma_{ys}}{J_{avg}} \tag{2}$$

where J_{avg} is the average J-integral along the crack front. $M = 30$ defines the specimen capacity limit in ASTM E1921. Based on the Master Curve, $M = 42$ was estimated to provide a typical median value at $T_0 - 20$ °C and $M = 75$ a typical median value at $T_0 - 50$ °C for miniature C(T) specimens.

In this study, the relative curvature is defined according to ASTM E1921-20 based on equation (1), where all the nine points along the crack front are applied. In the newest version of the standard, as explained earlier, only the seven innermost points are considered, therefore we also discuss the results in terms of ASTM E1921-21.

2.2. Material models

The material of the specimen is assumed to follow the elastic–plastic Ramberg-Osgood constitutive model (Equation (3)) with parameters given in Table 1. The loading pins (see Section 2.3) were considered elastic with the same elastic constants. As shown in Table 2, two strain hardening exponents were considered in the calculations.

$$\varepsilon = \frac{\sigma}{E} + \alpha \frac{\sigma}{E} \left(\frac{\sigma}{\sigma_0} \right)^{n-1} \tag{3}$$

2.3. Simulation models

Three-dimensional computational models were constructed to represent the considered crack front geometries using Abaqus finite element software version 2020. The models were used to calculate the J-

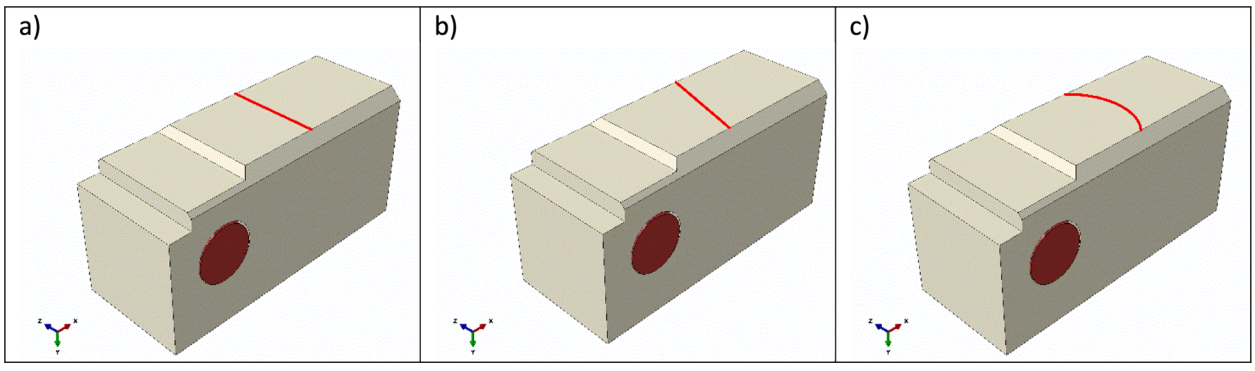

Fig. 1. Illustration of one half of a C(T) specimen with straight (a), slanted (b) and parabolic (c) crack fronts studied in the calculations. The maximum studied deviations from a straight front are visualized in (b) and (c).

Table 1
The different cases analyzed. SCF = straight crack front, PCF = parabolic crack front, SLCF = slanted crack front, b_0 = length of the ligament, J_{avg} = average J-integral along the crack front, B_N = specimen thickness accounting for the side-grooves, a_i = crack length at one of the nine measuring locations. M is the normalized inverse loading parameter. The depth of each side-groove is 10 % of the thickness.

Curvature type	Identification	Curvature, C, Equation (1) *	Strain hardening exponent, n	Yield stress, σ_0 [MPa]	Crack length, a_0 [mm]	M, Equation (2)
Straight	SCF M = 38	0	15	500	4	38
Straight	SCF M = 42	0	15	500	4	42
Straight	SCF M = 75	0	15	500	4	75
Parabolic	PCF M = 42C = 0.15	0.15 (0.07)	15	500	4.4	42
Parabolic	PCF M = 75C = 0.15	0.15 (0.07)	15	500	4.4	75
Parabolic	PCF M = 42C = 0.09	0.09 (0.05)	15	500	4.2	42
Parabolic	PCF M = 42C = 0.04	0.04 (0.03)	15	500	4.1	42
Straight	SCF n = 5 M = 42	0	5	500	4	42
Parabolic	PCF n = 5 M = 42C = 0.15	0.15 (0.07)	5	500	4.4	42
Slanted	SLCF M = 75C = 0.14	0.14 (0.10)	15	500	4	75

* In parentheses, we give the relative curvature defined according to ASTM E1921-21.

Table 2
Ramberg-Osgood parameters for the different materials.

	Elastic modulus E [GPa]	Poisson ratio ν	Yield offset parameter α	Yield stress σ_0 [MPa]	Hardening exponent (n)
Material 1	200	0.3	1.0	500	5
Material 2	200	0.3	1.0	500	15

integrals over the crack front and the stress fields in front of the crack tip needed for the constraint assessment. The models assume a fixed crack size, where the crack blunts as force is applied. The material properties and models used in the simulation were described in section 2.2. The loading was defined as quasi-static based on displacement of the loading pin. Symmetric boundary conditions were defined at the crack plane, and a frictionless contact between loading pin and specimen was assumed.

The models comprise a total of approximately 500 000 linear 3D reduced integration brick elements with a mesh size of 0.03 mm at the crack tip region, the number of nodes over the crack front exceeding 100. Fig. 2 shows the mesh in the crack tip region of the model with a parabolic crack shape. Large displacements (NLGEOM = YES in Abaqus) were considered to obtain an accurate representation of the crack tip stress state needed for the constraint calculations. The large deformation assumption does not affect the contour integral results evaluated further away from the crack tip with Abaqus contour integral routines. For each location on the crack front, the average of path-independent contours 5–10 were taken as the J-integral values. The crack mouth opening displacement (CMOD) was taken as the average of the crack mouth front face nodes.

2.4. Simulation results overview

This section presents the qualitative effect of the crack front shape on the stress and strain fields and the force–displacement behavior. The main results obtained in the simulations are the constraint parameters discussed in detail in Section 4. Fig. 3 shows the crack opening stress fields and the equivalent plastic strain contours for all three crack front

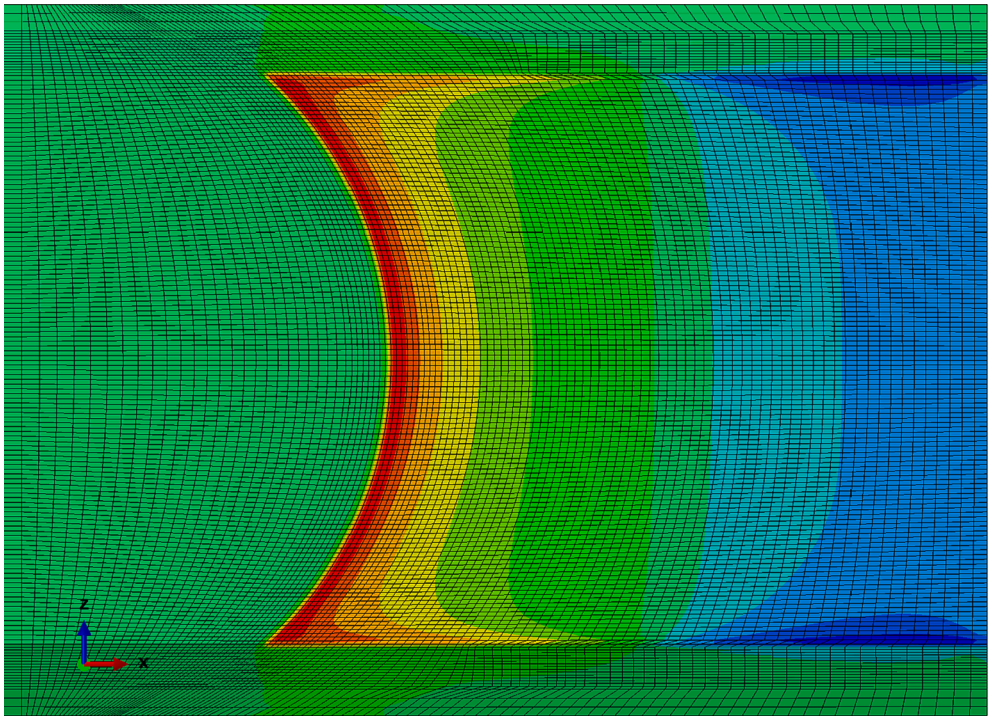

Fig. 2. Crack tip and plane mesh. Crack opening stresses are used as contour colors for illustration of the crack front location.

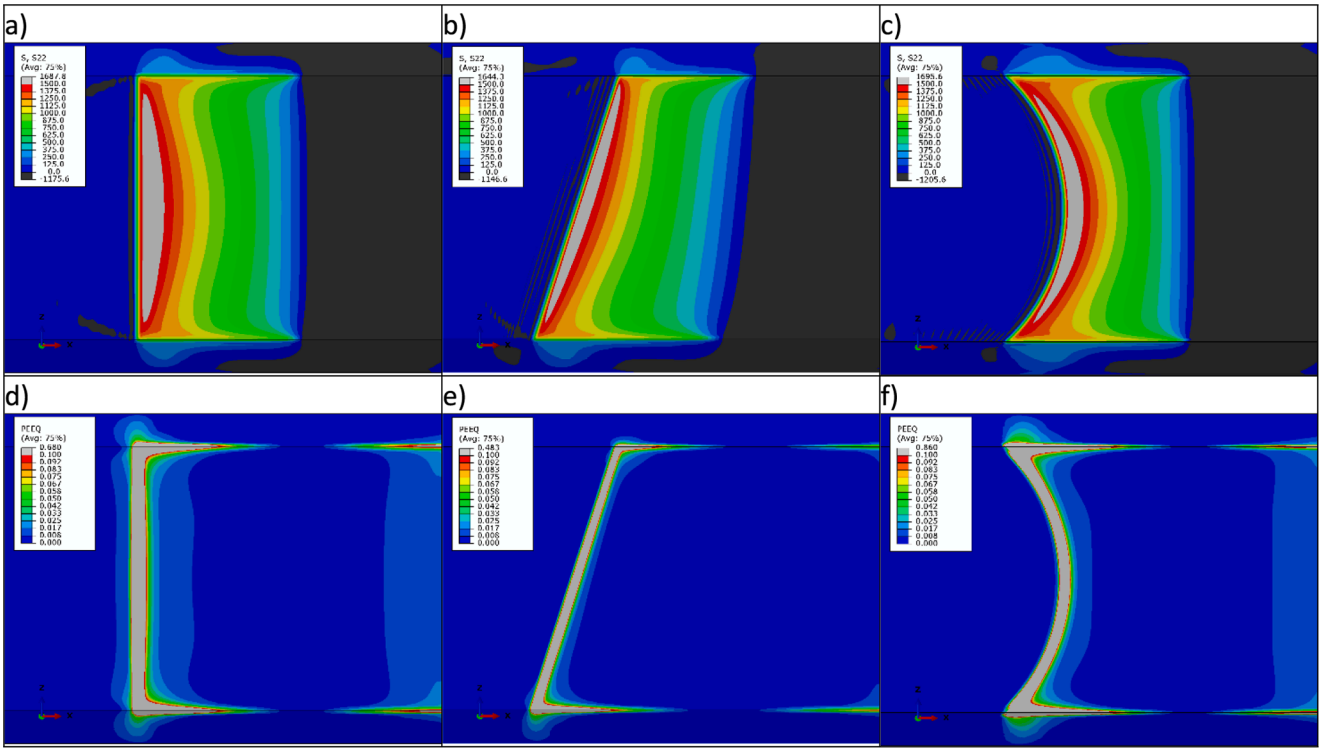

Fig. 3. Examples of the crack opening stress distribution (a-c) and equivalent plastic strain contours (d-f).

shapes at approximately J = 40 kJ/m^2 (M = 50). The normalized force and J-integral evolution as a function of normalized CMOD is plotted in Fig. 4.

In Section 4, the constraint parameter calculated from the simulation results is the Q-parameter [14], which is used for calculating the local failure probability based on the Master Curve as described in next section. The Q-parameter is defined as the normalized difference between the local crack opening stress σ_{22} field and a reference stress field:

$$Q = \frac{\sigma_{22}}{\sigma_0} - \frac{\sigma_{22,ref}}{\sigma_0} \tag{4}$$

The difference was evaluated at a normalized distance of $r_n = r\sigma_0/J = 2$. The direction and distance to the crack front, r, was taken in the primary crack growth direction, i.e. not considering local crack front curvature. The same assumption was made in the definition of the crack extension direction in the contour integral calculations. The reference field $\sigma_{22,ref}$ was calculated with a two-dimensional modified boundary layer model, as presented by [15]. The parameters given in Table 2 were used to calculate the reference stress field used in all locations over the crack front to calculate the Q-parameter.

2.5. Post-processing of the simulation results

The simulation data was post-processed to estimate the cumulative failure probabilities and the effect of curvature on T_0 for different temperatures relative to T_0. Cumulative failure probabilities were assessed based on the Master Curve procedure. The standard Master Curve cumulative failure probability, $P_{f,s}$, expression is of the form:

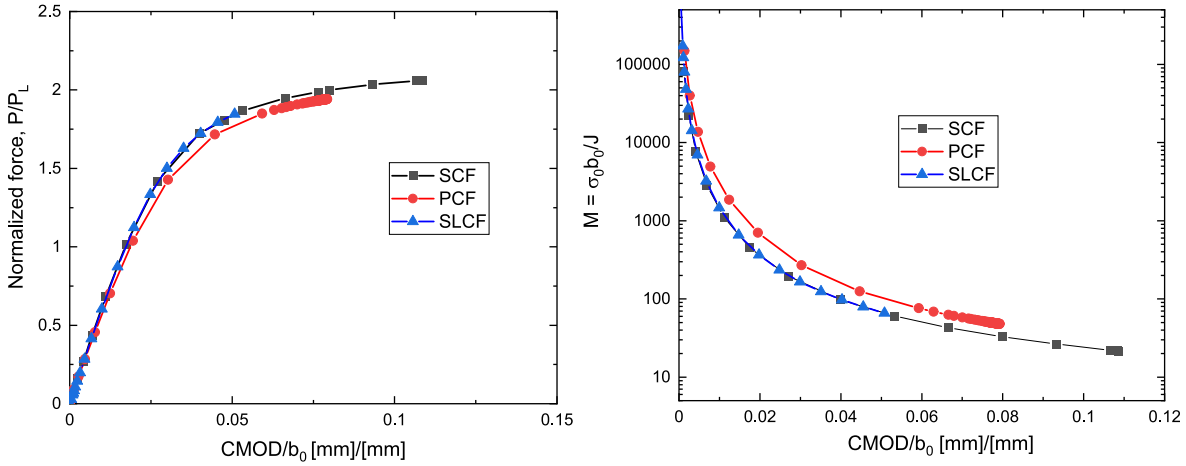

Fig. 4. a) Normalized CMOD, force, and b) J-integral data from the simulations with varying crack front curvature. The force was normalized with limit load for a C(T) specimen defined according to [13], where $P_L = 1.455\left(\sqrt{\left(\frac{2a_0}{b_0}\right)^2 + \frac{4a_0}{b_0} + 2} - \left(\frac{2a_0}{b_0} + 1\right)\right) Bb\sigma_0$.

$$P_{f,s} = 1 - exp\left\{ -\frac{B}{B_0}\left(\frac{K_J - K_{min}}{K_0 - K_{min}}\right)^4 \right\} \quad (5)$$

where B is the specimen thickness, B_0 is the reference specimen thickness, typically 25.4 mm, $K_{min} = 20MPa\sqrt{m}$, K_J is the stress intensity factor for a straight crack converted from J-integral by using expression:

$$J = \frac{K_J{}^2(1-\nu^2)}{E} \quad (6)$$

where E is Young's modulus and ν is Poisson's ratio, and

$$K_0 = 31 + 77exp(0.019(T - T_0)) \quad (7)$$

where T is the testing temperature and T_0 is the reference temperature. Equation (5) is based on the assumption that the constraint and the stress intensity factor are constant over the crack front, which is a reasonable assumption for C(T) and SE(B) specimens with straight crack fronts. K_J was based on J_{avg} along the crack front.

In reality, the local K_J, constraint and K_0 vary as a function of the location along the crack front (φ). In these situations, a more general expression for the cumulative failure probability, $P_{f,g}$, can be used, derived from Equation (5), [9]:

$$P_{f,g} = 1 - exp\left\{ -\int_0^S \left(\frac{K_{I\varphi} - K_{min}}{K_{0\varphi} - K_{min}}\right)^4 \frac{dS}{B_0} \right\} \quad (8)$$

where $K_{J\varphi}$ is the local stress intensity factor at location φ, $K_{0\varphi}$ is the local K_0 value, S is the length of the crack front, and dS is the length increment. The local K_0 value accounts for the constraint variation, [9,16,17]:

$$K_{0\varphi} = 31 + 77exp\left[0.019\left(T - T_{0,ref} + \Delta T_{0,constraint}\right)\right] \quad (9)$$

where $T_{0,ref}$ is the reference temperature, and, in this study, the temperature is the reference temperature for a C(T) specimen with a straight crack, and $\Delta T_{0,constraint}$ is the constraint correction for the reference temperature. The constraint dependence for T_0 in Equation (9) is based on work from [17]:

$$\Delta T_{0,constraint} = 40\left(Q_{ref} - Q_{local}\right) \quad (10)$$

Q_{local} is the local constraint parameter, and Q_{ref} is the reference constraint parameter for a straight crack resulting in $P_{f,s} = P_{f,g}$. In Section 4.2, where the Q and J-integral variations along the crack front are applied to estimate the cumulative probabilities along the crack front, equations (8) and (9) are applied. First the crack front is divided into increments and for each increment the function of the integral in equation (8) is solved locally. Finally, the incremental solutions are summed together. The problem can be solved analytically using a software program with spreadsheets.

3. Experimental methods and results

3.1. Materials and T_0 testing

Two different ferritic steels were investigated. The first material was a thermo-mechanically rolled, 25 mm thick ferritic steel plate, S460MC. The second material was a ferritic steel pipe (FP), 15NiCuMoNb5, typical of nuclear applications, with a thickness of 29 mm and an outer diameter of 376 mm. Fracture toughness testing was performed with miniature C(T) specimens, with nominal width, W, of 8 mm and thickness, B, of 4 mm, while the other dimensions conformed to ASTM E1921 [10]. The specimens were side-grooved after pre-fatigue, so that B_N = 3.2 mm.

The test matrix is presented in Table 3. The pre-crack surface of specimens extracted from the S460MC plate was normal to the rolling direction and the crack grew transverse to the rolling direction. The pre-crack surface of the specimens extracted from the FP pipe was normal to the axial direction of the pipe and the crack grew in the circumferential direction. The FP specimens were extracted from the mid-thickness of the pipe. The S460MC specimens were extracted from various locations in the through-thickness direction.

The testing was performed in accordance with ASTM E1921-20 [10]. The specimens were fatigue pre-cracked to target $a_0/W = 0.5$ using a RUMUL resonant testing machine. The testing was performed with a servo-hydraulic testing machine MTS 250kN, and inside an environmental chamber cooled using liquid nitrogen. The specimens were loaded at a quasi-static loading rate (in average 0.5 MPa $\sqrt{m}$/s) with monotonic displacement control until full fracture. Testing was carried out at a constant temperature close to the reference temperature T_0 estimated based on previous results. After testing, the specimens were immersed in liquid nitrogen to facilitate the breaking in two halves. To measure the final crack length, a traveling stage measuring microscope was used. The crack length was measured according to the 9-point measuring procedure as described in the Introduction.

3.2. Results

The T_0 and the relative crack front curvatures are presented in Table 4 for the materials. Fig. 5 presents the fracture toughness data. For material FP M_{avg}, is 71 and 130 for S460MC. The test temperatures for both materials were within the allowable temperature range of $T_0 \pm 50$ °C. Based on the inhomogeneity screening criterion in ASTM E1921, the FP material is macroscopically homogeneous, the second inhomogeneity screening iteration step provides the same T_0. Material S460MC is on the border of being characterized as macroscopically inhomogeneous.

The experimental data was processed to determine the curvature type. If maximum crack length was measured close to the surface (the first or the second outermost point) the crack front was defined as slanted. In one case, the crack was neither defined as parabolic nor slanted, since the lowest crack length was measured at the center, thus this data point was excluded from analysis. There are less slanted than parabolic crack fronts in the data sets, therefore, the detailed analyses focus more on the parabolic crack fronts. The transition temperature, T_0, for material S460MC is −106 °C and for FP −120 °C if only the PCFs are included.

For each data point with a PCF and M > 30, Fig. 6 shows the effect of curvature on the failure probability determined according to the Master Curve procedure, equation (5). The results are presented in this form, so that the effect of testing temperature can be neglected. The failure probabilities seem to be quite evenly distributed and independent of the curvature.

To investigate the effect of curvature on transition temperature in more detail, the data sets were divided into populations based on measured relative curvature as presented in Table 5. The average relative curvature in these populations varies between 0.05 and 0.11, but the T_0 does not change significantly. The variations in T_0 due to changes

Table 3
Test matrix; test temperature range, orientation, material, deformation behavior. Testing was done with miniature C(T) specimens.

Material	Identification	Number of specimens	Test temperature ° [C]	Orientation	Specimen	Strain hardening (n)	Yield strength [MPa]
S460MC	S460MC	44	between −100 and −150	L-T	4x8 C(T)	13	479
15NiCuMoNb5	FP	32	between −120 and −140	L-T	4x8 C(T)	13	504

Table 4
Transition temperature T_0 of studied series.

Material	Curvature type	Number of specimens	Curvature (C) range, equation(1)	Average Curvature*	Number of specimens above C = 0.1	Transition temperature T_0 °[C]
S460MC	PCF	38	0.04 – 0.15	0.08 (0.05)	10	−106
	SLCF	6	0.07 – 0.20	0.13 (0.10)	4	−96**
FP	PCF	20	0.04 – 0.20	0.08 (0.05)	5	−120
	SLCF	12	0.09 – 0.21	0.12 (0.09)	6	−121

* In parentheses, curvature estimate according to ASTM E1921-21.
** According to ASTM E1921, $\sum r \bullet n > 1$ should be fulfilled to get a valid T_0 estimate, where r is the number of uncensored data, and n is the specimen weighting factor. For the data set $\sum r \bullet n = 0.75$, the data set needs more results so that a valid T_0 can be determined.

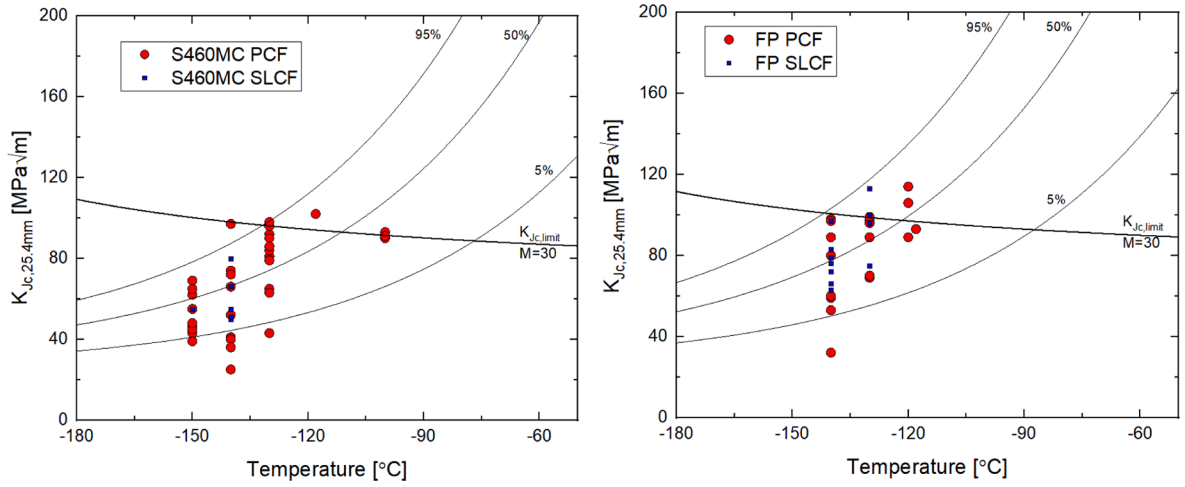

Fig. 5. Master Curves for material FP (left) and S460MC ferritic steel plate (right).

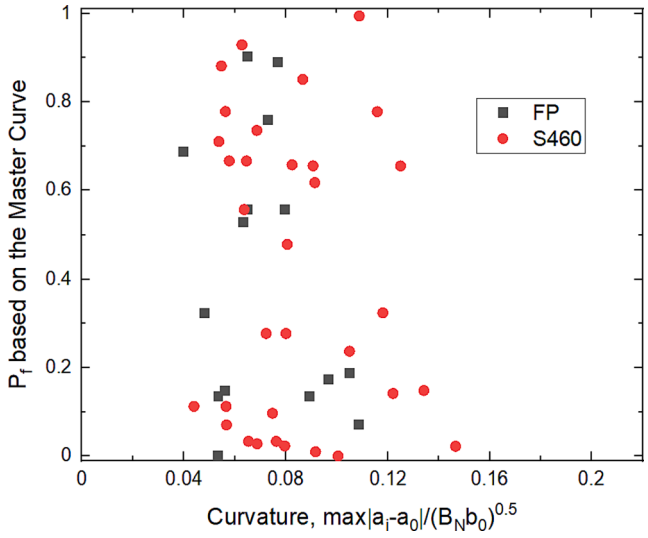

Fig. 6. Effect of curvature on failure probability. Only crack fronts defined as parabolic were included in the analysis. Only results with M > 30 are displayed.

in crack front curvature is −3 to + 3 °C. The standard deviation of T_0 for a typical data set is approximately 7 °C − 9 °C [7].

4. Discussion

4.1. Stress intensity and constraint profiles along the crack front

Fig. 7 compares the constraint (Q-parameter, [14]) profiles along the crack front for a straight (SCF), parabolic (PCF) with relative curvature C = 0.15 and slanted (SLCF) crack fronts with C = 0.14. For the SCF, the constraint profile changes with the normalized loading level M, equation (2). For higher relative loading, i.e. lower M-values, the constraint is marginally lower at the center and the drop in constraint is steeper towards the sides. Notably, the M-parameter is determined using J_{avg} and the remaining ligament b_0. Also for the PCF, the constraint decreases in the center with increasing loading, but the change in the profile is not as drastic. The Q-profile for the SLCF is mildly asymmetric but follows the Q-profile for the SCF.

Table 5
Effect of curvature on T_0.

Material	Curvature type	Average curvature (C)	Number of specimens	Number of specimens with M < 30	T_0 [°C]
S460MC	PCF	0.06	13	1	−107
		0.08	12	2	−104
		0.11	13	2	−106
FP	PCF	0.06	10	1	−118
		0.10	10	4	−121

Fig. 8 compares the K_J-profiles for the same cracks (PCF, SCF, SLCF), normalized by the K_J value at the center of the specimen. For the SCF, the stress intensity factor, K_J, reduces towards the side-groove. For a smaller loading (higher M-values), the stress intensity is more even along the crack front. The SLCF has a higher K_J-value on the side with the shorter local crack length. For the PCF, the K_J peaks close to the side-grooves where the crack is shorter. The $K_J/K_{J,center}$ ratio close to the side-grooves decreases as the loading increases.

The above K_J and Q profiles for the SCF are compared to a non-side-grooved C(T) specimen [3], Fig. 9 and Fig. 10. In [3], the Q and K_J

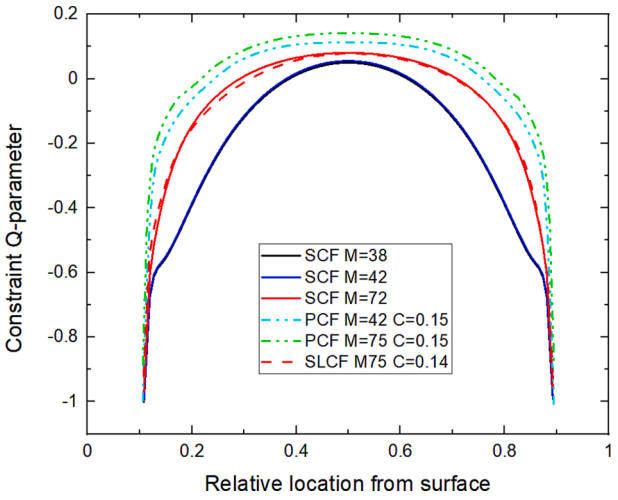

Fig. 7. Constraint variation along the crack for the different crack geometries. C is the curvature. The relative location in the figures gives the x-coordinate in thickness direction of the specimen. Relative locations 0.1 and 0.9 mark the root of the side-grooves and 0.5 gives the center of the specimen.

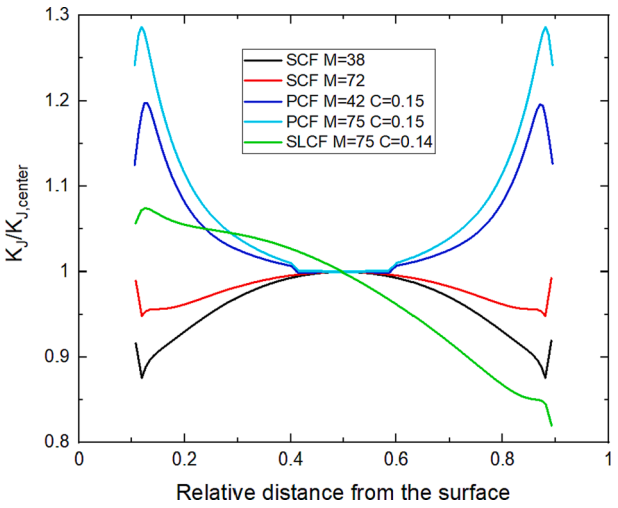

Fig. 8. Stress intensity profile along the crack front for the different crack geometries.

profiles are determined for a material with a yield strength of 585 MPa and n = 15. For the same relative loading levels, M = 40, the profiles follow approximately the same path up to the side-groove. For lower loading level, M = 200 and M = 75, the profile is flatter close to the center compared to M = 40.

The strain hardening parameter, n, was varied to estimate the effect on the stress intensity parameter, K_J, and constraint profiles, while the yield strength was kept at 500 MPa. The profiles for SCFs and PCFs are compared in Figs. 11 and 12 for n = 5 and n = 15. For the same level of curvature and M-parameter, the constraint is lower at the center when n = 5. The profiles are different, especially for PCF where the Q-value increases towards the surfaces of the specimen. The stress intensity profiles, Fig. 12, show that for the SCF when n = 5 the stress intensity is more even along the crack front, and for the PCF, the profile is more curved. The results suggest that both the stress intensity factor and Q-parameter profiles depend on the amount of plastic deformation at the crack tip, which in turn depends on the strain hardening exponent and a comparison of the profiles at equal M values is not fully descriptive. In the upcoming analyses, only the n = 15 results are further evaluated since those describe better the investigated materials.

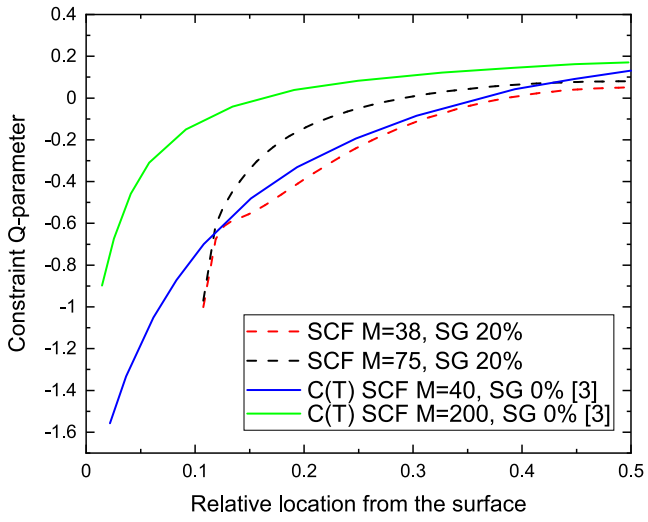

Fig. 9. Comparison of constraint behavior in the thickness direction of a C(T) specimen with side-grooves and without side-grooves and for different relative loading levels.

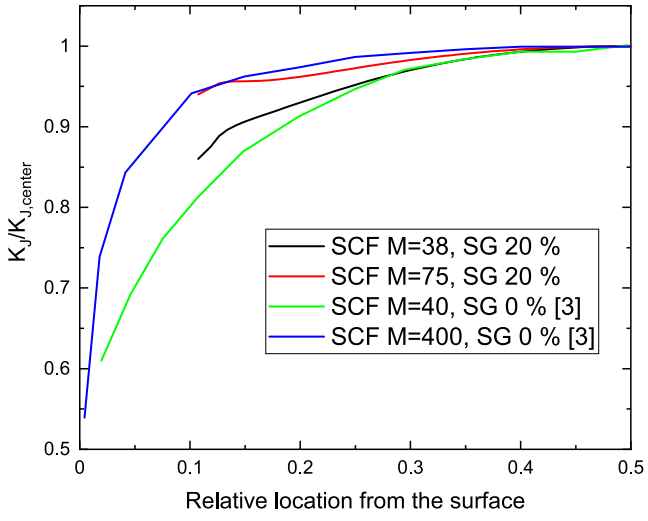

Fig. 10. K_J profiles for straight crack fronts. C(T) specimens with and without side-grooves.

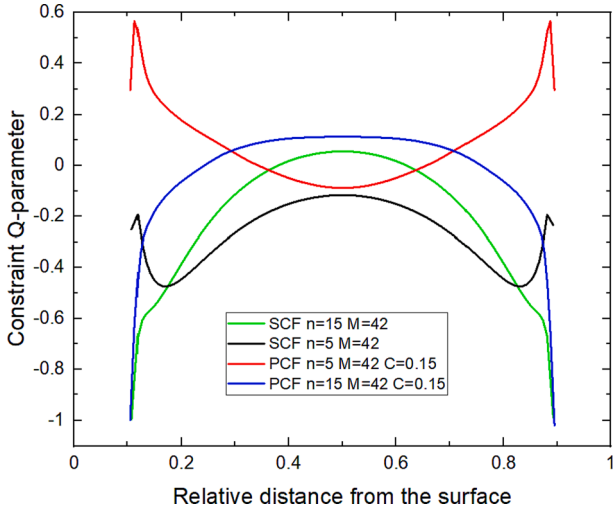

Fig. 11. Constraint profile comparison when n = 5 and n = 15.

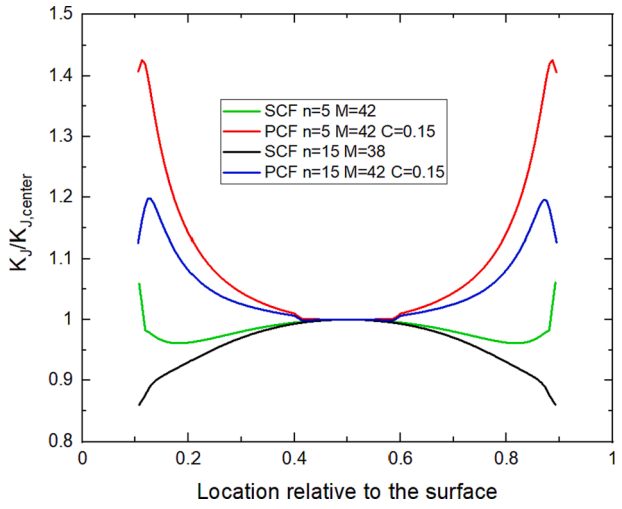

Fig. 12. Stress intensity factor profile comparison when n = 5 and n = 15.

4.2. Cumulative failure distributions

Fig. 13 shows an experimentally determined cumulative distribution for brittle failure initiation locations along the crack front. The distribution is based on investigations on initiation site locations along the crack front of side-grooved miniature C(T) specimens with $a_0/W = 0.5$. [3] In the figure, the experimental results are compared to the cumulative failure distribution calculated according to the method presented in Section 2.5, based on the simulation results from this study for the same specimen type and size. The cumulative distribution for M = 38 aligns with the experimental observation, indicating that brittle initiation is more likely in the central locations for a straight crack front than next to the side-grooves. For lower loading levels, M = 75, the cumulative failure probability distribution straightens, indicating more even local failure density along the crack front. Due to symmetry, a failure probability of 0.50 is reached at the center of the specimen. The result indicates that the applied method is capable to describe the physical behavior to some degree.

Fig. 14 compares cumulative failure distributions for a SCF, PCF and SLCF. The cumulative failure distribution profile for a SLCF crack front indicates a higher local failure density on the side with the shorter crack. At the center of the specimen, the cumulative failure probability is close

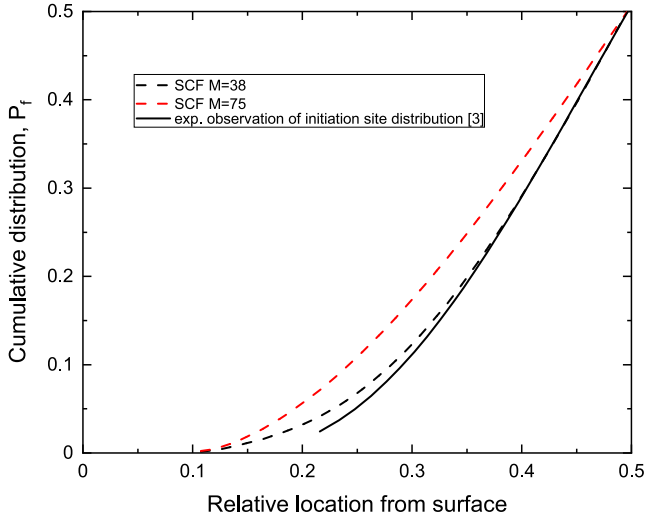

Fig. 13. Comparison of experimentally measured [3] and numerically determined cumulative distributions for initiation locations of brittle failure along the crack front.

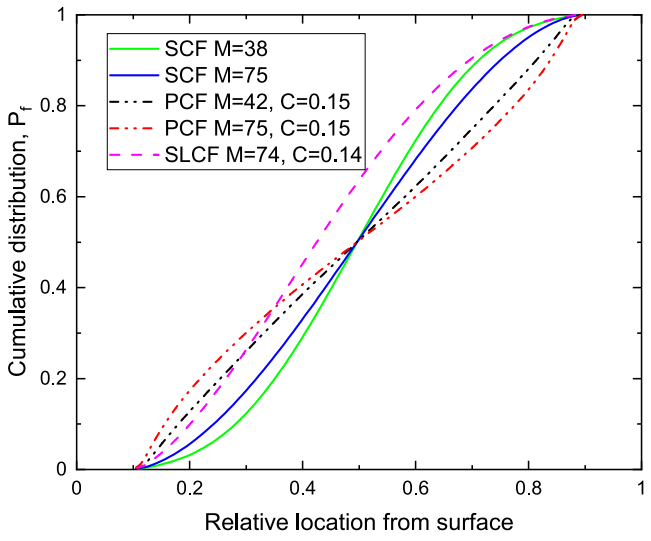

Fig. 14. Cumulative distributions for a SCF, SLCF and PCF.

to 0.6. For same normalized loading level, the profiles for the PCF indicate that the local failure density is more even along the whole crack front compared to the SCF case. The results for the PCF indicate that the susceptibility to failure might be higher closer to the surface. The cumulative distributions for a PCF and a SLCF cannot be validated since the effect of curvature on the failure density distribution has not been experimentally investigated previously. Additionally, the Q-parameter was estimated in the main crack growth direction. If the parameter is assessed perpendicular to the local crack front, the drop in Q will be larger close to the side-grooves and the susceptibility to failure will differ.

To assess the effect of curvature on T_0, Table 6 presents the estimated cumulative failure probabilities calculated for the different crack configurations at different median loading levels and temperatures relative to T_0. The results provide an initial estimate of possible trends investigated experimentally in Section 4.3. The failure probability, $P_{f,g}$, based on the general cumulative failure probability function, equation (8), was estimated using the local stress intensity factors and constraint values along the crack front. The failure probability, $P_{f,s}$, was estimated based on J_{avg} and the standard Master Curve cumulative failure probability

Table 6
Estimated effect of curvature on cumulative failure probability.

Crack front type	Relative temperature regime T-T_0 [°C]	$P_{f,g}$	$J_{avg,FEM}$ [kJ/m$_2$]	$P_{f,s}$ based on $J_{avg,FEM}$	Estimated change in T_0 [°C]
SCF M = 42	−20	0.36	48	0.36	
PCF M = 42 C = 0.15	−20	0.35	42	0.28	5.2
PCF M = 42 C = 0.09	−20	0.38	45	0.31	3.7
PCF M = 42 C = 0.04	−20	0.35	46	0.34	0.6
SCF M = 75	−50	0.44	27	0.44	
PCF M = 75 C = 0.15	−50	0.40	24	0.35	3.05
SLCF M = 74 C = 0.14	−50	0.46	27	0.45	0.7

distribution function, equation (5).

The results (Table 6) based on the applied method and assumptions indicate that for similar M-values the local variations in constraint and stress intensity factor do not have a significant impact on failure probability $P_{f,g}$ due to the curvature of the crack front. For similar M-values and for relatively high loading levels, M = 42, the failure probability $P_{f,g}$ stays quite close to 0.37. For lower loading, M = 75, of PCF, the effect of curvature appears to be marginal, $P_{f,g}$ varying from 0.44 to 0.40, and the estimated effect on T_0 being approximately 2 °C.

In practice according to ASTM E1921, the transition temperature assessment is based on an estimate of J_{avg} and the standard Master Curve cumulative failure probability distribution $P_{f,s}$. When the failure probability calculation is based on J_{avg} for a PCF, the resulting failure probability $P_{f,s}$ assuming a SCF is smaller than $P_{f,g}$, see Table 6. Since $P_{f,s} < P_{f,g}$, the effective stress intensity for the whole specimen is higher than K_J based on J_{avg}. Consequently, by basing the transition temperature assessment on J_{avg}, the resulting T_0 is estimated conservatively (Fig. 15). For the PCF with C = 0.15 and by basing the analysis on J_{avg}, the T_0 could be + 3 to + 5 °C higher, but this difference is still lower than the uncertainty in the T_0 estimate as defined in ASTM E1921-21. For a SLCF, the $P_{f,g}$ probability does not differ significantly from $P_{f,s}$, for M = 75.

One possible error source for curved crack fronts may come from calculating the J-integral according to ASTM E1921. Thus, the J_{avg} based on FEM was compared to J_{ASTM} determined according to ASTM E1921 from the simulated force-CMOD data at the same time step. Table 7 shows that the J_{avg} gives comparable values to J_{ASTM}, the error being less than 2 %. The simulated force-CMOD curves are presented in Fig. 4. Combined with the observation from Fig. 15, the results indicate that by basing the analysis on the $J_{avg} \approx J_{ASTM}$, a conservative T_0 estimate can be obtained for curved crack fronts.

Fig. 16 shows that the effect of curvature on compliance, C_0, for a C(T) specimen with a PCF is of the same order as for a SE(B) specimen with a PCF [11]. The compliance was determined from the slope in the elastic portion of the simulated force-CMOD curves and normalized by the compliance for a straight crack estimated according to ASTM E1921. For a SLCF, the effect of curvature on compliance is marginal, even for curvatures close to 0.15.

4.3. The effect of curvature on T_0

Fig. 17 compares the experimental data from Table 5 to the numerical linearized trends from Fig. 15. The results based on the numerical data and for the S460MC material indicate an increasing trend,

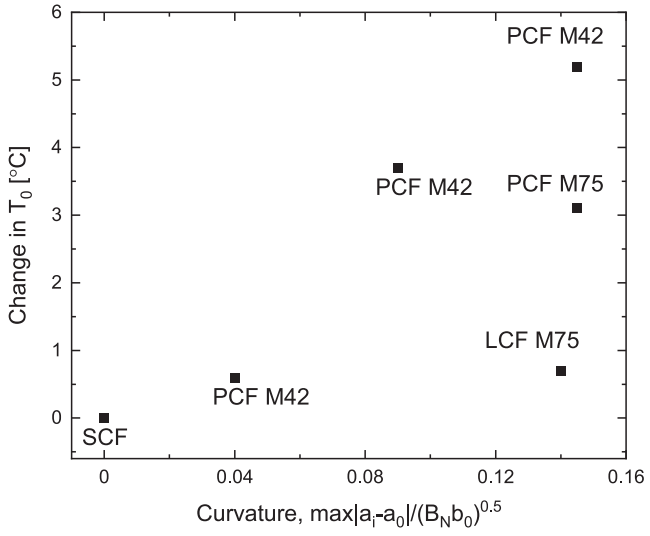

Fig. 15. Estimate of the effect of curvature on T_0. Analysis based on difference between $P_{f,g}$ and $P_{f,s}$ at a specific load level and relative temperature T-T_0.

Table 7
Comparison of the J-integral estimated from numerical data based on ASTM E1921 and obtained with FEM as an average along the crack front.

Case	J_{avg}(FEM) [kJ/m$_2$]	J_{ASTM} [kJ/m$_2$]	Difference [kJ/m$_2$]	Difference/ J_{avg}(FEM)
SCF M = 75	26.7	25.8	−0.9	−0.04
SCF M = 38	52.9	52.2	−0.7	−0.01
PCF M = 75 C = 0.15	32.1	31.7	−0.4	−0.01
PCF M = 42 C = 0.15	42.2	42.0	−0.2	−0.01
SLCF M = 74 C = 0.14	29.2	28.7	−0.5	−0.02

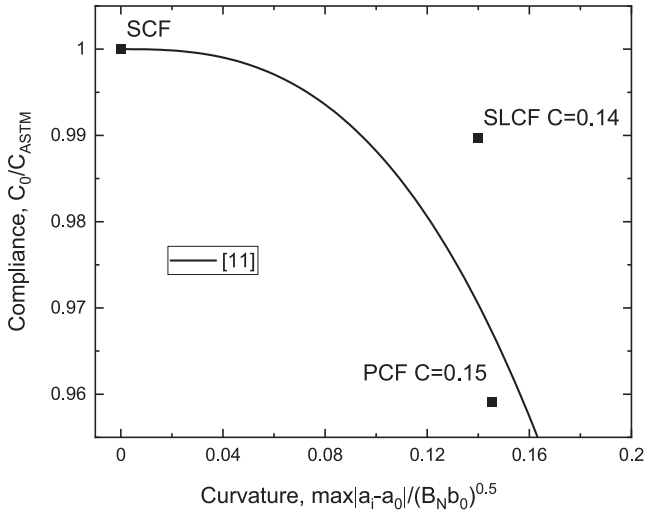

Fig. 16. Effect of curvature on compliance. The slope from [11] was developed for SE(B) specimens.

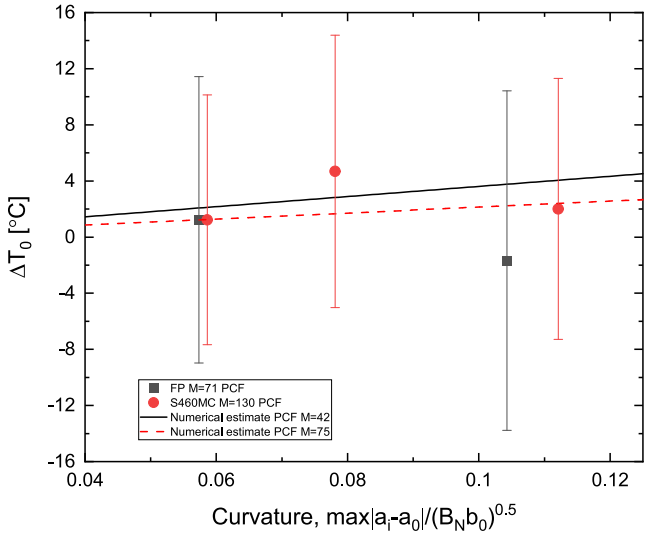

Fig. 17. Effect of crack curvature on T_0. The error bars display the 90 % confidence limit based on the uncertainty in the T_0 estimate due to sample size, as defined in ASTM E1921.

T_0 increases with increasing curvature. The results for the FP material point in the other direction. The trend of an increasing effect of curvature on T_0 is supported by data in [8], where T_0 was calculated based on data fulfilling the validity requirements of ASTM E1921-18 and a second T_0 was calculated based on data not fulfilling the crack front straightness requirement, i.e. for specimens with larger curvature. The invalid data

set contained 39 data points and the valid data set 12 points. A 8 °C higher T_0 is obtained in [8] with the invalid data. The results are affected by the uncertainty of the T_0 estimate.

Fig. 17 demonstrates the challenge with the quantification of the effect of curvature on fracture toughness in the ductile-to-brittle transition region based on experimental data. The same quantitative effect as obtained numerically is difficult to observe experimentally, since the possible effect of curvature on T_0 is smaller than the standard deviation of a typical T_0 estimate [7]. In addition, experimentally, the curvature of the crack front cannot be controlled. Thus, a sufficiently large data set is required, hopefully containing various curvatures. Ideally, the material should be macroscopically homogeneous to reduce one factor of uncertainty. Both materials in this investigation are characterized as macroscopically homogeneous according to the screening criterion in ASTM E1921.

Additional experimental data is required to validate the effect of crack front curvature on the reference temperature. Valuable data is obtained from ongoing European research project FRACTESUS (fracture mechanics testing of irradiated RPV steels by means of sub-sized specimens) focused on the development of miniature specimen techniques and STRUMAT (structural materials for nuclear safety and longevity), where miniature techniques are applied and validated [18,19]. Future work could also focus on analyzing the initiation site density along the crack front for PCFs with relative curvature above 0.1 to validate the numerical observations from this study.

As described in the beginning, the crack front straightness requirement in ASTM E1921 has changed during the last years. According to ASTM E1921-20 crack front straightness requirement, a PCF with C = 0.15 results in an invalid result. Based on the E1921-21 requirement, the relative curvature limit drops to 0.07 since the outermost points are excluded, i.e. the relative curvature is less than 0.1 and the result is valid. For the SLCF, C drops from 0.14 to 0.10. The results from this study support the development on relaxing the crack front straightness assessment, because for the investigated cases (C = 0–0.15), the effect of crack front curvature on the reference temperature is smaller than the uncertainty of the T_0 estimate, and the results point towards obtaining a more conservative (higher) T_0 estimate as the curvature increases.

5. Conclusions

The effect of crack front curvature on fracture toughness in the ductile-to-brittle transition region was investigated using numerical and experimental methods. In the numerical assessment, a 3D FEM model of a miniature C(T) specimen was constructed. The relative curvature, C, was varied between C = 0 and C = 0.15. Three types of crack front curvatures were investigated, straight (SCF), parabolic (PCF) and slanted (SLCF) crack fronts. The crack tip constraint and stress intensity factor at different locations along the crack front were determined. The numerical results were post-processed by applying the general cumulative failure probability method based on the Master Curve to estimate the possible effects of curvature on the reference temperature. The experimental T_0 testing was carried out on ferritic steels according to ASTM E1921-20 using miniature C(T) specimens. Based on the results, the following observations are made:

a. The results support the development on relaxing the relative curvature criterion in ASTM E1921. By increasing the crack front curvature, the numerical results indicate that T_0 tends to be more conservative. Experimental results show that as the curvature increases for PCFs from 0.06 to 0.11 the effect on T_0 is insignificant, −3 °C to + 3 °C, smaller than the uncertainty in the T_0 estimate.
b. The average J-integral obtained through numerical FEM simulations for curved crack fronts is of the same order as the J-integral calculated based on the equations in ASTM E1921-21.
c. Based on the numerical work for PCF with C = 0.15, the effect on T_0 is +5 °C compared to a straight crack front when M = 42, and +3 °C when M = 75. For similar M-values, the effect of curvature on failure probability is insignificant when the local variations in stress intensity factor and constraint are accounted for. The largest effect of curvature on T_0 comes from basing the calculations on the average J-integral along the crack front neglecting the local variations in constraint and J-integral.
d. For slanted crack fronts based on the numerical assessment, the effect of curvature on T_0 appears to be smaller than for parabolic crack fronts.

Future research should focus on analysis of the effect of curvature on fracture toughness for other materials, preferably large experimental data sets with varying crack front curvatures and materials with varying stress strain behavior. The methods applied in this work provide a basis for future analyses.

CRediT authorship contribution statement

S. Lindqvist: Methodology, Conceptualization, Formal analysis. **J. Kuutti:** Methodology, Writing – review & editing.

Declaration of Competing Interest

The authors declare the following financial interests/personal relationships which may be considered as potential competing interests: Both authors, Sebastian Lindqvist and Juha Kuutti, work at VTT which is a non-profit research organization. The work has been conducted for the SAFIR2022 research program focusing on nuclear safety. The results can be applied for standard and method development.

Acknowledgements

The research is part of project AMOS (Advanced Materials Characterisation for Structural Integrity) that is funded through SAFIR2022 (The Finnish Research Programme on Nuclear Power Plant Safety 2019 - 2022).

References

[1] K. Wallin, T. Planman, M. Valo, R. Rintamaa, Applicability of miniature size bend specimens to determine the master curve reference temperature T 0, Eng. Fract. Mech. 68 (11) (2001) 1265–1296.
[2] M. Valo, T. Planman, K. Wallin, R. Ahlstrand, J. Kohopää, R. Rintamaa, Validationn of miniature fracture toughness specimens for material surveillance, Small specimen test techniques: Fourth Volume (2002) 18–32.
[3] K. Wallin, M. Yamamoto, U. Ehrnstén, Location of initiation sites in fracture toughness testing specimens - the effect of size and side grooves. PVP2016 2016: 1–9.
[4] M. Yamato, K. Onizawa, Y. Kentaro, T. Ogawa, Y. Mabuchi, M. Valo, et al., International round robin test on master curve reference temperature evaluation utilizing miniature C(T) specimens, Small specimen test techniques: 6th volume 2015;6:53–69.
[5] R. Chaouadi, E. van Walle, M. Scibetta, R. Gérard, On the use of miniaturized CT specimens for fracture toughness characterization of RPV materials, Proc ASME 2016 Press Vessel Pip Conf (2016) 1–10.
[6] K. Wallin, The master curve method: A new concept for brittle fracture, Int. J. Mater. Prod. Technol. 14 (1999) 342–354.
[7] ASTM E1921-21. Standard test method for determination of reference temperature, To, for ferritic steels in the transition range; 2021.
[8] M. Lambrecht, R. Chaouadi, M. Li, I. Uytdenhouwen, M. Scibetta, On the possible relaxation of the ASTM E1921 and ASTM E1820 Standard specifications with respect to the use of the mini-CT specimen, Mater. Perform. Charact. 9 (2020) 593–607, https://doi.org/10.1520/MPC20190217.
[9] K. Wallin, Use of the Master Curve methodology for real three dimensional cracks, Nucl. Eng. Des. 237 (2007) 1388–1394, https://doi.org/10.1016/j.nucengdes.2006.09.034.
[10] ASTM E1921-20. Standard Test Method for Determination of Reference Temperature, To, for Ferritic Steels in the Transition Range. ASTM Int 2020.
[11] Z. Yan, Investigation of fracture toughness measurement for pipeline steels based on SE (B) and SE (T) specimens. Western University, 2014.
[12] ASTM E1921-18. Standard test method for determination of reference temperature, To, for ferritic steels in the transition range, 2018.
[13] T.L. Anderson, Fracture mechanics: Fundamentals and applications, 3rd ed. Taylor & Francis Group, LLC, 2005.

[14] N.P. O'Dowd, C.F. Shih, Family of crack-tip fields characterized by a triaxiality parameter-i. structure of fields, J. Mech. Phys. Solids 39 (8) (1991) 989–1015.
[15] M. Kroon, J. Faleskog, H. Öberg, A probabilistic model for cleavage fracture with a length scale - Parameter estimation and predictions of growing crack experiments, Eng. Fract. Mech. 75 (2008) 2398–2417, https://doi.org/10.1016/j.engfracmech.2007.08.009.
[16] S. Lindqvist, K. Wallin, Master curve procedure accounting for the combined; 2019, pp. 1–7.
[17] M. Moattari, I. Sattari-Far, Modification of fracture toughness Master Curve considering the crack- tip Q -constraint, Theor. Appl. Fract. Mech. 90 (2017) 43–52, https://doi.org/10.1016/j.tafmec.2017.02.012.
[18] Horizon 2020. FRACTESUS (Fracture mechanics testing of irradiated RPV steels by means of sub-sized specimens). https://snetp.eu/portfolio-items/fractesus/. Accessed: 1.7.2022; 2020.
[19] Horizon 2020. EU-project STRUMAT (Structural materials for nuclear safety and longevity). https://strumat-lto.eu/background/. Accessed: 1.7.2022 2020.